HEAT 2008, Fifth International Conference on
Transport Phenomena In Multiphase Systems
June 30 - July 3, 2008, Bialystok, Poland

3D CFD Calculation of Injector Nozzle Model Flow for Standard and Alternative Fuels

L. Perković[1], D. Greif[2], R. Tatschl[2], P. Priesching[2], N. Duić[1]

[1]Faculty of Mechanical Engineering and Naval Architecture, University of Zagreb, Croatia; luka.perkovic@fsb.hr, neven.duic@fsb.hr
[2]AVL List GmbH, Hans List Platz 1, A-8020, Graz, Austria; david.greif@avl.com, reinhardt.tatschl@avl.com, peter.priesching@avl.com

ABSTRACT

In this work multi phase flow and erosion analysis were done via simulations in AVL's Workflow Manager with FIRE Solver CFD application, for standard diesel and two alternative biofuels, FAME and DME, inside different nozzle models and with various boundary conditions. Driving force for fluid flow is static pressure difference between inlet and outlet. Analysis criteria were: phase volume fraction distribution due to cavitation, mass flow rate, absolute velocity profile vs. nozzle model narrow channel height and erosion MDPR. Nozzle model consists of narrow channel with sharp (type I) or rounded (type Y) inlet section, with or without downstream placed target, so there was a total of four different model geometries. Simulation results showed that cavitation was present in almost all cases and that clear difference between three observed fuels can be seen. Mass flow in channel type I was lower than one in channel type Y. When comparing three observed fuels, it was noticed that DME fuel usually had highest velocity, but lowest mass flow rate. Contrary to DME, FAME fuel showed highest mass flow rate despite lowest velocity.

When designing fuel nozzles, cavitation and cavitation erosion should always be considered. Nozzles in which less cavitation occured, achieved higher mass flow rates for same boundary conditions. When comparing simulation results and physical properties of observed fuels, it can be concluded that density is a leading term in determining mass flow rate. Also, erosion model predicts more intensive MDPR value near narrow channel exit.

INTRODUCTION

In this project it was planned to analyze multi phase cavitating flow for different kind of model nozzles, especially focusing on the type of fuel which is used. Standard diesel fuel was under investigation as well as different alternative fuels, DME and FAME. Since the physical properties of these biofuels differ significantly from the fuels used nowadays, it was necessary to analyze them on different nozzle models.

Advantage of CFD approach is in fact that it can represent characteristics of the flow field in a single nozzle hole, which is generally unknown and not accessible for measurements (Badock et al., 1999). Even with transparent nozzles in original size the optical access by shadowgraph technique is difficult because of the total reflection by cavitation films lying around the liquid (Badock et al., 1997; Chaves et al., 1995). The laser light sheet technique enables a view of the core of the flow which is covered by cavitation films and not visible with shadowgraph (Badock et al., 1999). Neutron radiography is suitable for visualizing the fuel behaviors inside the metallic nozzle (Takenaka et al., 2005). Investigation of cavitation phenomena showed that for nearly all the duration of the injection process the nozzle injector hole is surrounded by cavitation films (Eifler, 1990).

The AVL's Workflow Manager with FIRE Solver CFD application (hereafter AVL FIRE) offers the possibility to simulate multi phase flow situations like they are appearing in all kind of fuel injection nozzles.

At the beginning, a brief overview of mathematical model is presented. Important equations regarding to multi phase models are given. After defining parameters of mathematical model, computational domain is presented. It consists of nozzle model mesh with corresponding boundary and initial conditions. Next, fuel properties table is given for all three observed fuels. Results, are divided into two groups, one calculated with nozzle models with (Target cases) and other without (Channel cases) downstream placed target.

When labeling phases in two-phase flow, liquid phase will be labeled as continuous phase or phase 01 and gas phase will be labeled as dispersed phase or phase 02.

MATHEMATICAL MODEL

Mathematical model was set up for quasi-stationary, inner, non-compressible, viscous, turbulent and two-phase type of flow. Simulations were done using *Multiphase* module. In *Multiphase* module *Multifluid* model is used, which means that equations for all phases are calculated separately, with pressure as only coupled variable. Volume fraction of total must be equal to one. It consists of fundamental fluid dynamic conservation equations, *k-ε* turbulence model equations and interfacial models equations. For interfacial mass exchange Linear Cavitation Model was used and for interfacial momentum exchange Cavitation Drag Model was used. Both interfacial exchange models imply two additional transport equations: Bubble Number Density and Interfacial Area equation. These equations bring up additional closure coefficients of mathematical model. The erosion model follows the work of Berchiche et al., 2002, and Franc & Riondet, 2006, and provides two variables: Erosion Incubation Time and Mean Depth of Penetration Rate (MDPR).

Turbulent Kinematic Viscosity of Continuous Phase

As shown in Eq. (1) turbulence kinematic viscosity consists of bubble induced turbulence (BI) and shear induced turbulent viscosity (SI).

$$\nu_c^t=\nu_c^{t,SI}+\nu_c^{t,BI} \tag{1}$$

Equation (2) is used for calculating bubble induced turbulence (Sato and Sekaguchi, 1975).

$$\nu_c^{t,BI}=C_{Sato}D_b\left|\overrightarrow{v_r}\right|\alpha_d \tag{2}$$

The relative velocity is defined as:

$$\overrightarrow{v_r}=\overrightarrow{v_d}-\overrightarrow{v_c} \tag{3}$$

Linear Cavitation Model

Mass exchange can be derived to be equal to:

$$\Gamma_c=\frac{1}{C_{CR}}\text{sign}(\Delta p)3.85\frac{\rho_d}{\sqrt{\rho_c}}\left(N'''\right)^{\frac{1}{3}}\left(\alpha_d\right)^{\frac{2}{3}}\left|\Delta p\right|^{\frac{1}{2}}=-\Gamma_d \tag{4}$$

where the effective pressure difference equals:

$$\Delta p=p_{sat}-\left(p-C_E\frac{2}{3}\rho_c k_c\right) \tag{5}$$

Cavitation Drag Model

Interfacial momentum source includes drag and turbulent dispersion forces, Eq (6).

$$\overrightarrow{M_c}=C_D\frac{1}{8}\rho_c A_i'''\overrightarrow{v_r}\left|\overrightarrow{v_r}\right|+C_{TD}\rho_c k_c\nabla\alpha_d=-\overrightarrow{M_d} \tag{6}$$

Drag coefficient C_D, Eq. (8), is a function of the bubble Reynolds number, Eq (7).

$$Re_b=\frac{v_r D_b}{\nu_c} \tag{7}$$

$$C_D=\begin{cases}\dfrac{192}{Re_b}\left(1+0.1Re_b^{0.75}\right) & Re_b\leq 1000\\ 0.438 & Re_b>1000\end{cases} \tag{8}$$

Bubble Number Density and interfacial Area Equations

In order to account for the variable size nature of the bubble distribution, this model uses interfacial area , Eq. (9), and number density, Eq. (10), transport equations, derived from Moment method solution of Liouville's theorem.

$$\frac{\partial N'''}{\partial t}+\nabla\cdot\left(N'''\overrightarrow{M}\right)=\sum R_j+R_{ph} \tag{9}$$

$$\frac{\partial A'''}{\partial t}+\nabla\cdot\left(A'''\overrightarrow{M}\right)=\sum \Phi_j+\Phi_{ph} \tag{10}$$

Source terms on right-hand side of the previous equations have been discussed by Ishii et al. (2003), Sun et al. (2004) for two-phase bubbly flows and by Yao et al. (2004) for gas-liquid boiling flows.

Equations (11) and (12) represent coalescence due to random collision

$$R_{rc}=4.4\cdot 10^{-3}C_{rc}\frac{\varepsilon^{\frac{1}{3}}A^{\frac{11}{3}}}{\alpha\alpha_{max}^{\frac{2}{3}}}\left[1-\exp\left(-C_{rc}\frac{\alpha^{\frac{1}{3}}\alpha_{max}^{\frac{1}{3}}}{\alpha_{max}^{\frac{1}{3}}-\alpha^{\frac{1}{3}}}\right)\right] \tag{11}$$

$$\Phi_{rc}=-0.17C_{rc}\frac{\varepsilon^{\frac{1}{3}}\alpha^{\frac{1}{3}}A^{\frac{5}{3}}}{\alpha_{max}^{\frac{1}{3}}\left(\alpha_{max}^{\frac{1}{3}}-\alpha^{\frac{1}{3}}\right)}\left[1-\exp\left(-C_{rc}\frac{\alpha^{\frac{1}{3}}\alpha_{max}^{\frac{1}{3}}}{\alpha_{max}^{\frac{1}{3}}-\alpha^{\frac{1}{3}}}\right)\right] \tag{12}$$

where α_{max} is the maximum volume fraction related to the packing limit, taken to be 0.62.

Equations (13) and (14) represent breakup due to turbulent impact

$$R_{ti}=5.2\cdot 10^{-3}C_{ti}\left(1-\alpha\right)\frac{\varepsilon^{\frac{1}{3}}A'''^{\frac{11}{3}}}{\alpha^{\frac{8}{3}}}\exp\left(-\frac{We_{c,ti}}{We}\right)\sqrt{1-\frac{We_{c,ti}}{We}} \tag{13}$$

$$\Phi_{ti}=0.12C_{ti}\varepsilon^{\frac{1}{3}}\left(1-\alpha\right)\frac{\varepsilon^{\frac{1}{3}}A'''^{\frac{5}{3}}}{\alpha^{\frac{2}{3}}}\exp\left(-\frac{We_{crit,ti}}{We}\right)\sqrt{1-\frac{We_{crit,ti}}{We}} \tag{14}$$

where We_{crit} is the critical Webber number, taken to be 2.3.

Equations (15) and (16) represent bubble generation due to phase change.

$$R_{ph}=C_{ph}\frac{6Ph}{\rho\pi D_{nuc}^3} \tag{15}$$

$$\Phi_{ph}=C_{ph}\frac{6Ph}{\rho D_{nuc}} \tag{16}$$

Following equation represents closure equation of interfacial mass and momentum transfer:

$$Ph=\text{sign}(\Delta p)\frac{\rho_d}{\sqrt{\rho_c}}\left(N'''\right)^{\frac{1}{3}}\left(\alpha_d\right)^{\frac{2}{3}}\left|\Delta p\right|^{\frac{1}{2}} \tag{17}$$

Closure Coefficients and Empirical Factors

In order to close mathematical model, AVL FIRE user interface enables user to enter values for closure coefficients and empirical factors. Model equations label, as well as GUI label with used value, are given in Table 1.

Table 1 Closure coefficients and empirical factors of mathematical model

Label in model equations	*GUI label*	*Value*
C_E	Egler factor	1.2
C_{CR}	Condensation reduction factor	10
C_{rc}	CC1	1
C_{ti}	CB1	0.1
C_{ph}	CB4	1
D_{nuc}	CB5	1e-006
C_{Sato}	Sato's coefficient	0.6
C_{TD}	Dispersion coefficient	0.5

COMPUTATIONAL DOMAIN

Nozzle Model Geometries With Corresponding Meshes

We have a total of four different nozzle model geometries. In all models narrow channel represents fuel injector nozzle. There are narrow channel models with sharp (type I) and rounded (type Y) inlet, Fig. 1, without downstream placed target. Cases, where no target is present in model geometries were labeled as Channel cases.

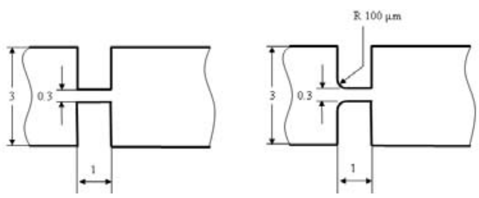

Fig. 1 Narrow channel type I (left) and type Y (right) geometries

Another nozzle models are those which have downstream placed target, Fig. 2, and which also have narrow channel type I or Y with same geometry as presented in Fig. 1. Cases with targets will be labelled as Target cases. Purpose of target is upstream influence on narrow channel flow, similar to influence of cylinder on flow inside real injector nozzle.

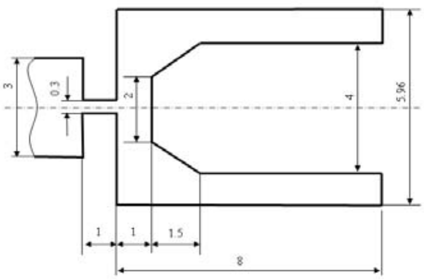

Fig. 2 Target position and geometry

Depth of all models is 0.3 mm. Geometry of nozzle model is symmetrical regarding to x-y plane so computational domain consists from half of nozzle model geometry, regarding to x-y plane, Fig. 3. As a result of that, mesh thickness in all cases, determined with z coordinate, is equal to 0.15 mm.

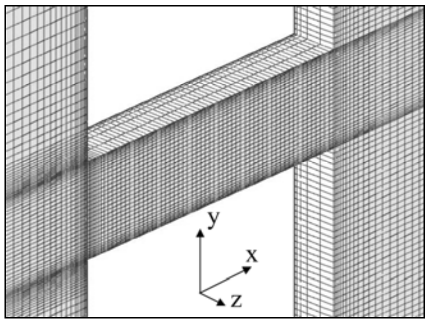

Fig. 3 Narrow channel detail with orientating coordinates

Selections and Boundary Conditions

All computational domains, representing nozzle model geometries, have four different boundary selections used to define boundary conditions: fluid inlet and outlet, symmetry plane and erosion surfaces. Inlet and outlet boundaries are presented in Table 3. If there was no specific selection made, boundary is assumed to be a wall.

Pressure, which is coupled variable, is defined only for continuous phase, Table 2. In order to achieve calculation stability, flow direction is defined on inlet boundary.

Table 2 Boundary conditions of static pressure

Model case	*Inlet (MPa)*	*Outlet (MPa)*
Channel	10	4
	20	8
	30	8
	30	12
	40	16
Target	10	0.1
	40	2

Table 3 Inlet and outlet boundary conditions

Selection	*Variables*	*Continuous phase*	*Dispersed phase*
Inlet	static pressure	depends on case	-
	flow direction	x=1, y=0, z=0	-
	turbulent kinetic energy	0.1	0.3
	turbulent length scale	2e-04	2e-04
	turbulent dissipation rate	25	125
	volume fraction	0.99999	1e-06
Outlet	static pressure	depends on case	-
	turbulent parameters are not fixed	-	-
	volume fraction	0.99999	1e-06

Table 4 Physical properties of observed fuels

				Diesel	DME	FAME
Phase 1	density	ρ	kg/m^3	828	661	880
	dynamic viscosity	μ	Pas	2.14E-03	1.558E-04	3.52E-03
	saturation pressure	p_{sat}	Pa	892	892 (assumption)	892 (assumption)
Phase 2	density	ρ	kg/m^3	7	11.23	11.5
	dynamic viscosity	μ	Pas	1E-05	1.028E-05	1E-05 (assumption)

Initial Conditions and Time Parameters

Initial conditions were: in every cell velocity was set to zero and static pressure was set to be equal to pressure on inlet selection. Since flow type was expected to be quasi-stationary, small variations of mass flow rates were expected. Simulation time step is 1e-08 s, and simulation end time is 4e-07 s.

PHYSICAL PROPERTIES OF OBSERVED FUELS

Physical properties for all observed fuels are listed in Table 4. Properties for FAME are from a book ‘Biodiesel’ by M. Mittelbach.

Properties of FAME fuel are similar to mineral diesel, while properties of DME are similar to liquefied natural gas, Semelsberger et al. (2006).

RESULTS

Analysis Criteria and Result Representation

For all cases there is unique result presentation and analysis criteria.

Analysis criteria for volume fraction distribution due to cavitation are cavitation length and thickness. Cavitation distribution was taken from x-y symmetry plane, Fig. 3, around narrow channel area. Very important analysis criteria is mass flow rate achieved in narrow channel, which is critical zone for fluid flow. It was taken from inlet selection to avoid mass accumulation due to phase change. Continuous phase absolute velocity profiles vs. narrow channel height were taken near narrow channel exit along line that lies on x-y symmetry plane. Erosion MDPR was taken on erosion selections, which are located on narrow channel upper and lower wall, perpendicular to symmetry plane.

Nozzle Models Without Downstream Placed Target

In Fig. 6 continuous phase volume fraction distribution can be seen for three different pressure drops. Cavitation occurs in all Channel type I cases and it is longest and thickest in FAME fuel cases. In Channel type Y cases cavitation is negligible, except in 30-08 MPa pressure drop case.

Mass flow is presented in Figures 4 and 5 for all pressure drops. FAME fuel achieves highest mass flow rates in all cases. DME has lowest mass flow rates. Generally, mass flow rates in Channel Y cases are higher than ones in Channel I cases for same boundary conditions.

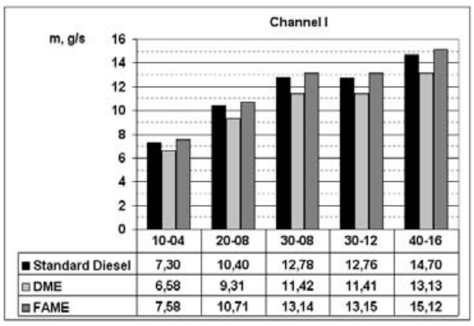

Fig. 4 Mass flow rates in Channel I cases for all pressure drops

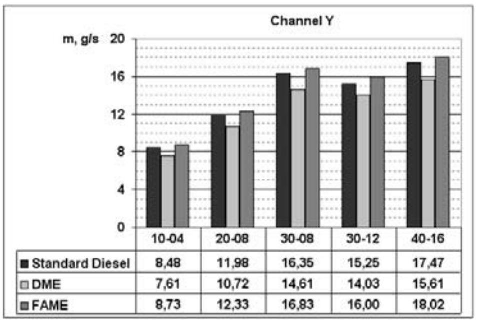

Fig. 5 Mass flow rates in Channel Y cases for all pressure drops

Velocity profile vs. channel height in Figures 7 and 8 shows that DME fuel achieved highest velocities in all cases, and that in Channel cases type I flow is rather undeveloped. In Channel Y cases flow velocity profiles are showing same trend regarding to fuel type, but flow is developed here, Fig. 9.

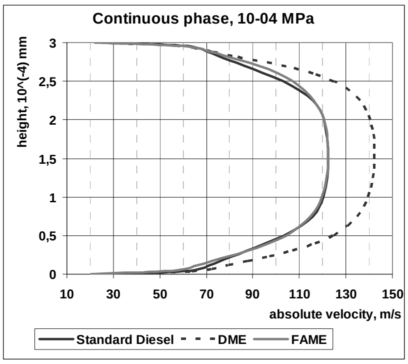

Fig. 7 Velocity profiles vs. narrow channel height in Channel I 10-04 MPa pressure drop case

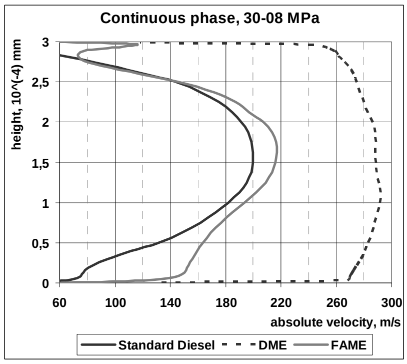

Fig. 8 Velocity profiles vs. narrow channel height in Channel I 30-08 MPa pressure drop case

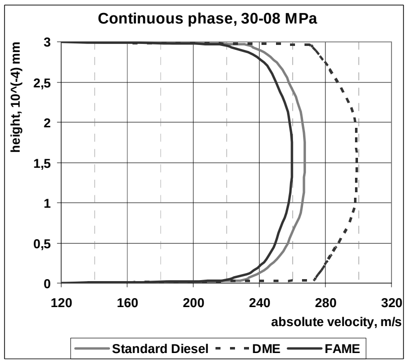

Fig. 9 Velocity profiles vs. narrow channel height in Channel Y 30-08 MPa pressure drop case

Erosion MDPR distribution, which is presented in Fig. 10, is also shown for three pressure drops. It can be noticed that for Channel cases type I MDPR is greater in near narrow channel exit. In Channel cases type Y greater values of MDPR are also present near rounded narrow channel inlet.

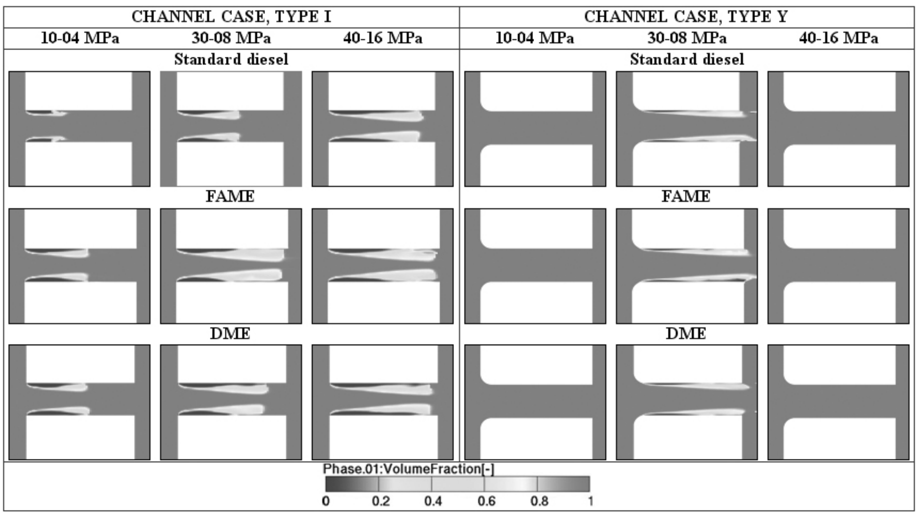

Fig. 6 Continuous phase volume fraction distribution in Channel cases

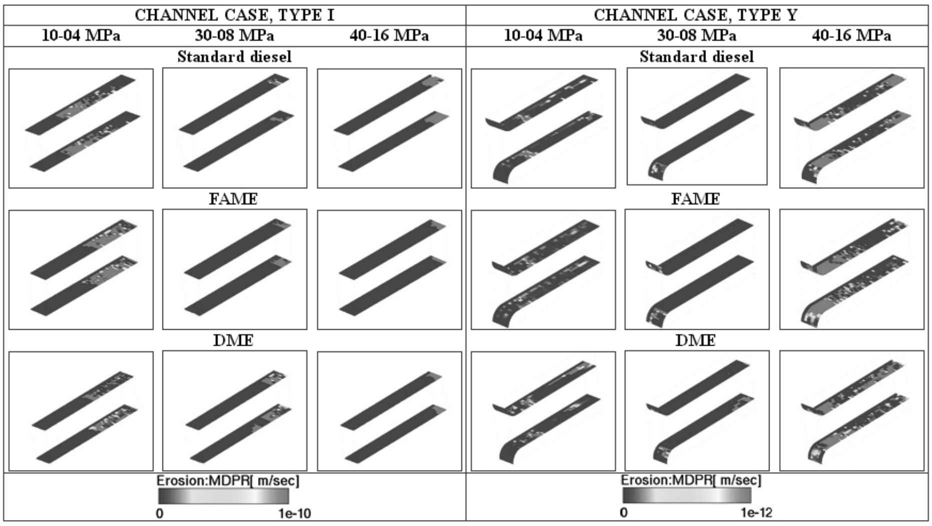

Fig. 10 Erosion MDPR distribution along narrow channel wall in Channel cases

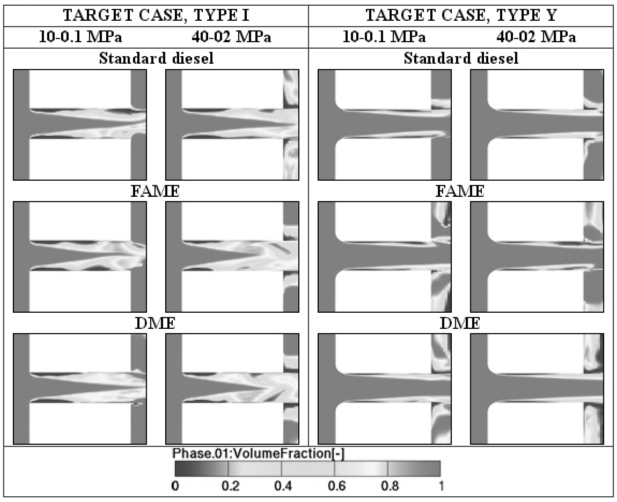

Fig. 11 Continuous phase volume fraction distribution in Target cases

Nozzle Models With Downstream Placed Target

In Fig. 11 continuous phase volume fraction distribution for all Target cases is presented. Cavitation occurs in all cases along whole narrow channel, but cavitation streams are much more thinner in Target cases type Y.

Mass flow is presented in Fig.12, and it shows same trend as in previous chapter. Again FAME fuel achieves highest and DME fuel lowest mass flow rates in all cases, and again mass flow rates in Target Y cases are higher than ones in Target I cases for same boundary conditions.

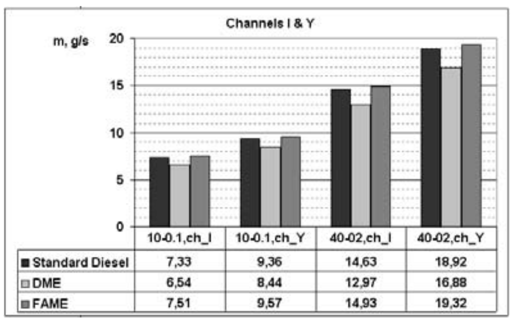

Fig. 12 Mass flow rates in Target cases for all cases

Velocity profiles vs. channel height are presented in Figures 13-16. Again DME achieved highest velocities in all cases. It is noticeable that flow is much more developed in Target I cases, than it is in Channel I cases.

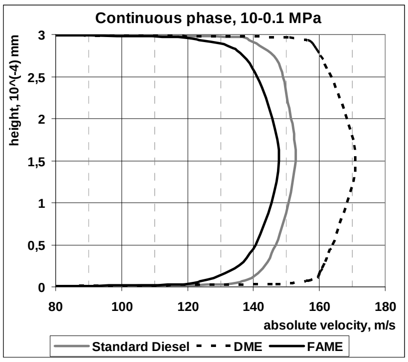

Fig. 13 Velocity profiles vs. narrow channel height in Target I 10-0.1 MPa pressure drop case

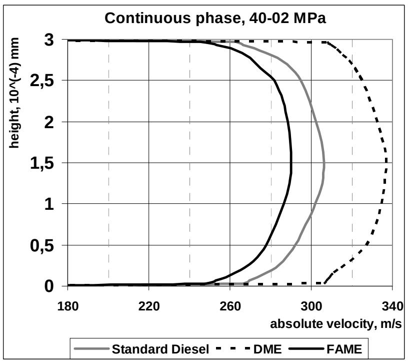

Fig. 14 Velocity profiles vs. narrow channel height in Target I 40-02 MPa pressure drop case

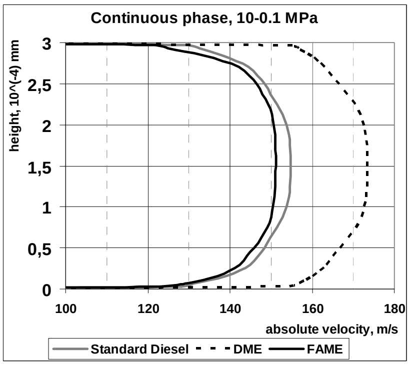

Fig. 15 Velocity profiles vs. narrow channel height in Target Y 10-0.1 MPa pressure drop case

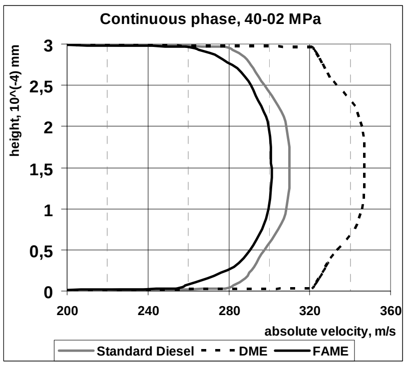

Fig. 16 Velocity profiles vs. narrow channel height in Target Y 40-02 MPa pressure drop case

Erosion MDPR, Fig. 17, shows that DME fuel has highest MDPR value close to the narrow channel exit. In Target Y cases it can be seen that erosion is more intense near rounded narrow channel inlet.

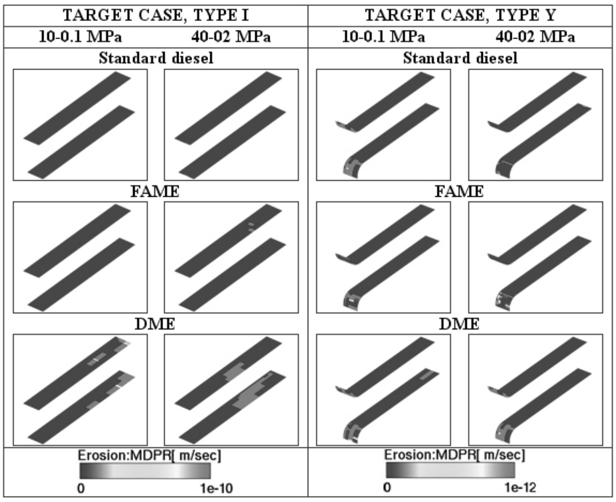

Fig. 17 Erosion MDPR distribution along narrow channel wall in Target cases

CONCLUSIONS

Most significant conclusion when comparing all fuels is regarded to their mass flow rates. When looking Figures 4, 5 and 12 and taking Table 4 into consideration, it can be noticed that fluid density is more significant property than viscosity. This is concluded upon a fact that in almost all cases DME fuel had highest velocity, which is generally related to viscosity, but lowest mass flow rate due to lowest density. FAME fuel Standard diesel and FAME had similar results due to their similar properties. Their mass flow rates were higher than DME's which is related to their greater density.

When comparing Figures 4, 5 and 12 with Figures 6 and 11, following conclusion imposes. Nozzles in which less cavitation occurs inside narrow channel, which is critical region for nozzle mass flow rate, will achieve larger mass flow rates for same boundary conditions.

Based on simulation results, when designing fuel nozzles, cavitation should always be considered as well as resulting cavitation erosion. As presented in Figures 6 and 11, cavitation is significantly reduced with rounded narrow channel inlet. Also, when comparing Figures 10 and 17, it can be seen that downstream placed target reduces MDPR inside narrow channel wall. This means that condensation of dispersed phase occurs outside narrow channel region, probably on target.

NOMENCLATURE

A'''	interfacial area density	1/m
D_b	bubble diameter	m
D_{nuc}	nucleate bubble size	m
k	specific kinetic energy	m^2/s^2
M	linear momentum	$kg/(m\ s)^2$
MDPR	Mean Depth of Penetration Rate	m/s
N'''	bubble number density	$1/m^3$
p	pressure (static)	Pa
Ph	term representing closure Eq. 17	$kg/(m^3\ s)$
R_j	number density source term not related to phase change	$1/(m^3\ s)$
R_{ph}	number density source term related to phase change	$1/(m^3\ s)$
t	time	s
v	velocity	m/s
α	volume fraction	m^3/m^3
Γ	interfacial mass exchange	$kg/(m^3\ s)$
ε	turbulent dissipation rate	m^2/s^3
ν	kinematic viscosity	m^2/s
ρ	fluid density	kg/m^3
Φ_{ph}	interfacial area source term related to phase change	1/(m s)
Φ_j	interfacial area source term not related to phase change	1/(m s)
C_{CR}	condensation reduction factor	-
C_E	Egler coefficient	-
C_{ph}	closure coefficient	-
C_{rc}	closure coefficient	-
C_{Sato}	Sato's coefficient	-
C_{ti}	closure coefficient	-
Re	Reynolds number (defined in Eq. 7)	-
We	Webber number	-
We_{crit}	Critical Webber number	-

Subscripts

c	continuous phase
d	dispersed phase
D	drag
i	interfacial
j	source terms not related to phase change
ph	source terms regarding to phase change
r	relative between dispersed and continuous
sat	saturation
TD	turbulent dispersion

Superscripts

BI	bubble induced
SI	shear induced
t	turbulent

REFERENCES

AVL FIRE v.8 Manual, Multiphase flow, July 2007

Badock, C., Wirth, R., Fath, A., Leipertz, A., 1999, Investigation of cavitation in real size diesel injection nozzles, *International Journal of Heat and Fluid Flow,* Vol. 20, pp. 538-544

Berchiche, N., Franc, J.P., Michel, J.M., 2002, A Cavitation Erosion Model for Ductile Materials, *Journal of Fluids Engineering*, Vol. 124, pp. 601-606.

Franc, J.P. and Riondet, M., 2006, Incubation Time and Cavitation Erosion Rate of Work-Hardening Materials, *Sixth International Symposium on Cavitation CAV2006*, Wageningen, The Netherlands

Greif, D., Morozov, A., Winklhofer, E., Tatschl, R., 2005, Experimental and numerical investigation of erosive effects due to cavitation within injection equipment, *Proc. of 4th International Conference on Computational Heat and Mass Transfer*, Paris-Cachan, France, Paper reference No: ICCHMT'05 – 257

Ishii, M., Sun, X. and Kim, S., 2003, Modeling strategy of the source and sink terms in the two-group interfacial area, *Annals of Nuclear Energy*, Vol. 30, pp. 1309-1331

Semelsberger, T.A., Borup, R.L., Greene, H.L., 2006, Dimethyl Ether (DME) as an Alternative Fuel, *Journal of Power Sources*, Vol. 156, pp. 497-511

Sun, X., Kim, S., Ishii, M., Beus, S., 2004, Modeling of bubble coalescence and disintegration in confined upward two-phase flow, *Nuclear Engineering and Design*, Vol. 230, 3-26

Takenaka, N., Kadowaki, T., Kawabata, Y., Lim, I.C., Sim, C.M., 2005, Visualization of cavitation phenomena in a Diesel engine fuel injection nozzle by neutron radiography, *Nuclear Instruments and Methods in Physics Research*, A 542, pp. 129–133

Yao, W. and Morel, C., 2004, Volumetric interfacial area prediction in upward bubbly two-phase flow, *International Journal of Heat and Mass Transfer*, Vol. 47, pp.307-328